Epitaxial Metal Halide Perovskites by Inkjet-Printing on Various Substrates

Mykhailo Sytnyk, Amir-Abbas Yousefi-Amin, Tim Freund, Annemarie Prihoda, Klaus Götz, Tobias Unruh, Christina Harreiss, Johannes Will, Erdmann Spiecker, Jevgen Levchuk, Andres Osvet, Christoph J. Brabec, Ulrike Künecke, Peter Wellmann, Valentin V. Volobuev, Jędrzej Korczak, Andrzej Szczerbakow, Tomasz Story, Clemens Simbrunner, Gunther Springholz, Daniel Wechsler, Ole Lytken, Sebastian Lotter, Felix Kampmann, Janina Maultzsch, Kamalpreet Singh, Oleksandr Voznyy, and Wolfgang Heiss*

Metal-halide-perovskites revolutionized the field of thin-film semiconductor technology, due to their favorable optoelectronic properties and facile solution processing. Further improvements of perovskite thin-film devices require structural coherence on the atomic scale. Such perfection is achieved by epitaxial growth, a method that is based on the use of high-end deposition chambers. Here epitaxial growth is enabled via a ≈1000 times cheaper device, a single nozzle inkjet printer. By printing, single-crystal micro- and nanostructure arrays and crystalline coherent thin films are obtained on selected substrates. The hetero-epitaxial structures of methylammonium $PbBr_3$ grown on lattice matching substrates exhibit similar luminescence as bulk single crystals, but the crystals phase transitions are shifted to lower temperatures, indicating a structural stabilization due to interfacial lattice anchoring by the substrates. Thus, the inkjet-printing of metal-halide perovskites provides improved material characteristics in a highly economical way, as a future cheap competitor to the high-end semiconductor growth technologies.

1. Introduction

Metal-halide-perovskites (MHPs) are the most promising material system for next-generation photovoltaics,[1,2] which exhibits the fastest annual increase of record power conversion efficiency observed so far.[3,4] This rapid evolution of performance is enabled by numerous research groups, working on improvements in perovskite material compositions, microstructures, morphologies, and interface engineering.[3–9] It is obvious that the performance of solar cells and other electronic devices crucially depends on defects, present in bulk, and increasingly at surfaces and grain boundaries. Hence, single-crystal devices usually outperform polycrystalline and amorphous ones, which is also observed for

Dr. M. Sytnyk, A.-A. Yousefi-Amin, T. Freund, Prof. W. Heiss
Institute – Materials for Electronics and Energy Technology (i-MEET)
Department of Materials Science and Engineering
Friedrich-Alexander-Universitat Erlangen-Nürnberg
Energy Campus Nürnberg
Fürtherstraße 250, Nürnberg 90429, Germany
E-mail: Wolfgang.Heiss@fau.de

A. Prihoda, Dr. K. Götz, Prof. T. Unruh
Institut für Physik der Kondensierten Materie
Friedrich-Alexander-Universitat Erlangen-Nürnberg
Staudtstr. 3, Erlangen 91058, Germany

A. Prihoda, Dr. K. Götz, Prof. T. Unruh, C. Harreiss,
Dr. J. Will, Prof. E. Spiecker
Center for Nanoanalysis and Electron Microscopy
Friedrich-Alexander University of Erlangen-Nuremberg
Cauerstraße 3, Erlangen 91058, Germany

A. Prihoda, Dr. K. Götz, Prof. T. Unruh, C. Harreiss,
Dr. J. Will, Prof. E. Spiecker
Interdisciplinary Center for Nanostructured Films
Friedrich-Alexander University of Erlangen-Nuremberg
Cauerstraße 3, Erlangen 91058, Germany

C. Harreiss, Dr. J. Will, Prof. E. Spiecker
Institute of Micro- and Nanostructure Research
Department of Materials Science and Engineering
Friedrich-Alexander University Erlangen-Nürnberg
Cauerstrasse 6, Erlangen 91058, Germany

Dr. J. Levchuk, Dr. A. Osvet, Prof. C. J. Brabec,
Dr. U. Künecke, Prof. P. Wellmann
Institute-Materials for Electronics and Energy Technology
Department of Materials Science and Engineering
Friedrich-Alexander-Universitat Erlangen-Nürnberg
Martensstraße 7, Erlangen 91058, Germany

Dr. V. V. Volobuev, J. Korczak, Dr. A. Szczerbakow, Prof. T. Story
Institute of Physics
Polish Academy of Sciences
Aleja Lotnikow 32/46, 02–668 Warsaw
Poland and International Research Centre MagTop
Aleja Lotnikow 32/46, Warsaw 02-668, Poland

MHPs.[10–18] Furthermore, also other important properties, such as environmental stability, charge transport, and carrier lifetimes, are superior in single crystals as compared to polycrystalline materials.[19–21] The most advanced process to obtain single crystalline films for electronic device fabrication is epitaxial growth (epitaxy means ordered growth on top of a crystalline substrate). While epitaxy from vapors is standard for conventional inorganic semiconductors such as silicon, germanium, or III/V compounds,[22–26] it has been recently also obtained for MHPs.[27,28] Chemical vapor deposition of $CH_3NH_3PbCl_3$ on mica substrates[29] and $CsPbBr_3$ on $SrTiO_3$[30] was successfully shown, as well as molecular beam epitaxy of $CsSnBr_3$ on NaCl substrates.[27] Coherent and continuous films were demonstrated in an interesting attempt called "remote epitaxy," using polar substrates coated with graphene, to obtain epitaxial halide perovskite films with improved carrier lifetimes.[28] A special feature of the metal-halide-perovskite is that they allow processing from solutions. Therefore, the spin coating was introduced to obtain in particular $CH_3NH_3PbI_3$ crystallites on KCl substrates, exhibiting superior light detectivity as compared to any other crystalline or a polycrystalline structure from the same material.[31] Recently, the spin coating was expanded as a general method to obtain epitaxial nano-microstructures from ionic crystals, such as sodium chloride, zinc oxide, lead iodide, and the MHP $CsPbBr_3$.[32] Here, we introduce inkjet-printing as a versatile technology for the epitaxial growth of MHP from tiny amounts of liquid precursors. Drop-on-demand (DOD) inkjet printing is a digital, additive, and very flexible printing technique, not only used in offices to print on paper, but also for the cost-effective fabrication of different devices and electronic systems. In the past, it has been applied for the printing of electrodes,[33,34] high-performance field-effect transistors and circuits,[35,36] memory devices,[36] sensors,[37,38] and thin-film solar cells.[39,40] An advantage of the inkjet printing is certainly

that the materials are deposited with picoliter amounts on predefined locations on the substrate so that the printing process is highly material-economic. This is advantageous in respect to the spin coating, where all the substrate area is covered, and lots of material is flung from the substrate during deposition. Besides, the composition and structure of the printed layers can be easily and rapidly tuned by mixing separate inks from multichannel print-heads. It was shown that inkjet printing could result in "single-crystal" structures from organic semiconductors.[41] However, these structures did not have any epitaxial relation to the substrate and would be better called crystalline domains. In comparison to that, here, the MHPs were deposited on crystalline substrates, enabling the continuation of the substrates atomic lattice by the deposited epitaxial layer. This is the main feature of epitaxial growth, which is usually performed in high-cost deposition chambers. Epitaxial structures are starting materials for the fabrication of high-end electronic devices such as lasers, light emitting diodes, high mobility transistors, micro-electro-mechanical systems, or radio frequency transducers, all required by the huge and rapidly growing electronic market. While the classical epitaxial growth on substrate wafers uniformly covers the whole substrate, epitaxial growth by inkjet printing offers the possibility to obtain the precise deposition of epitaxial structures just at the positions on the substrates, where they are needed for further processing. Thus, the inkjet printing is highly material economic and the equipment needed for that deposition, here we use a single nozzle device with some driver electronics, is about 100 to 1000 times cheaper than a classical epitaxial deposition system, based on ultra-high vacuum chambers and thermal evaporators. What remains is to find conditions on how to achieve such an epitaxial growth, rather than an uncontrolled crystallization on the crystalline substrates. Consequently, a required feature as an indication for epitaxial growth, is that all the deposited material is of crystalline nature, as is evidenced by crystal shapes and facets, and all formed structures have the same orientation on the substrate. The so far unsolved question is how to obtain such structures by inkjet printing. While parameters like lattice mismatch, substrate temperature, and possibly deposition rates are known to be crucial from classical high vacuum deposition, it is still a question if these parameters are sufficient to obtain epitaxy from inkjet printing. In the following the epitaxial growth of the archetypical MHPs, $CH_3NH_3PbBr_3$, $CH_3NH_3PbI_3$, (CH_3NH_3 = methyl ammonium, MA), $CsPbBr_3$, and $CsPbCl_3$ is discussed. As a result, we found Pb-chalcogenides as the most promising substrates to achieve epitaxial MHPs. This choice for the substrates was also guided by our previous work on the formation of epitaxial ligand shells from perovskites onto colloidal PbS nanocrystals. In particular, bismuth iodide and lead iodide based perovskites were found to offer suitably small lattice mismatch to PbS to provide shells with good crystalline properties.[42] As a novel parameter for epitaxy, environmental humidity is shown to be of crucial importance, as well as proper activation of the surface of the substrate. Furthermore, the epitaxial single-crystalline structures show similar optical properties as perovskite single-crystals, evidencing their high quality. The advantage of the epitaxial system is not only that they are deposited in thin films, which is advantageous for further device fabrication, but

Dr. V. V. Volobuev
National Technical University "KhPI"
Kyrpychova Str. 2, Kharkiv 61002, Ukraine

Dr. C. Simbrunner, Prof. G. Springholz
Institute of Semicondcutor and Solid State Physics
Johannes-Kepler-Universität Linz, Linz 4040, Austria

Dr. C. Simbrunner
E + E Elektronik Ges.m.b.H.
Langwiesen 7, Engerwitzdorf 4209, Austria

D. Wechsler, Dr. O. Lytken
Lehrstuhl für Physikalische Chemie II
Friedrich-Alexander-Universität Erlangen-Nürnberg
Egerlandstraße 3, Erlangen D-91058, Germany

S. Lotter, F. Kampmann, Prof. J. Maultzsch
Chair of Experimental Physics
Department of Physics
Staudtstraße 7, Erlangen 91058, Germany

F. Kampmann
Institute of Solid-State Physics
Technische Universität Berlin
Hardenbergstr. 36, Berlin 10623, Germany

K. Singh, Prof. O. Voznyy
Clean Energy Lab
Department of Physical & Environmental Sciences
University of Toronto Scarborough
Toronto M1C 14A, Canada

also that their cubic lattice structure is stabilized by the substrate because it is maintained over an extended temperature range. Thus, epitaxy by inkjet printing offers economic, environmental, and technical reasons, including, low cost, material effectivity, high-quality materials, and improved stability to apply this technology for any solution-processed semiconductor. The MHPs demonstrated here are a showcase example, however, the method has the potential to be applied to a large variety of semiconductors for electronic device developments.

2. Results and Discussion

2.1. Epitaxy of MAPbBr3 by Inkjet Printing

The special approach toward epitaxial growth in this paper is that it was achieved by inkjet printing. For printing, a single glass nozzle with an orifice of 80 μm was used, allowing the ejection of single droplets of the precursor solutions with a concentration of 0.25 M in dimethyl-formamide (DMF)/dimethyl-sulfoxide (DMSO) 3:1 onto substrates (**Figure 1**A top panel). As for classical techniques, a key toward epitaxial growth is the choice of a suitable substrate, as well as the proper selection of the substrate temperature (Figure S1, Supporting Information). For all following experiments, the substrates were heated to 80 °C, measured on the substrates surface by an attached thermo-element. This temperature was sufficient for solvent drying. The substrate was moved under the nozzle by a constant speed, so that the resulting pattern (single droplets

with various distances (Figure S2, Supporting Information) or merged to form a line with undulated borders) was controlled by the ejection frequency. The crystallization of the MHPs was checked by confocal-optical or scanning electron microscopy of dried samples, which was completed by a second heating step, performed at 100 °C in nitrogen atmosphere. Figure 1 shows printed methyl ammonium lead bromide (MAPbBr$_3$) perovskite. Printing on cleaned glass substrates, (Figure 1B top) or on GaAs wafers without removal of the natural oxide layer (Figure 1B middle) resulted in spots covered by crystallites of the MHPs. The crystallites exhibited random shapes and orientations, due to the amorphous structure of the substrates surface. Epitaxial growth requires substrates with crystalline surfaces, and a lattice matching to the deposited material. Thus, we have chosen here PbS single crystals as substrate, exhibiting a cubic lattice similar as that of the MAPbBr$_3$, with a lattice parameter difference of only 0.3% (Figure 1A bottom). The single crystals were freshly cleaved, and their surface was activated by etching in a bromine solution in methanol for 5 s. As proven by X-ray photoelectron spectroscopy (XPS), the etching removes oxygen and adds Br$^-$ ions (Figure S3, Supporting Information). By slightly sputtering the surface, the Br- ions are completely removed, suggesting that Br- binds to surface Pb atoms only. Thus, the Br- ions form an ordered interlayer, on which the nucleation of Pb^{2+} and MA$^+$ cations occurs. The etching with a Br$^-$ solution was found to be an essential step to obtain any epitaxial growth on Pb-chalcogenide substrates (Figures S4, Supporting Information). Inkjet printing of MAPbBr$_3$ on such prepared PbS (100) surfaces resulted in rectangular shaped and well faceted crystallites, randomly
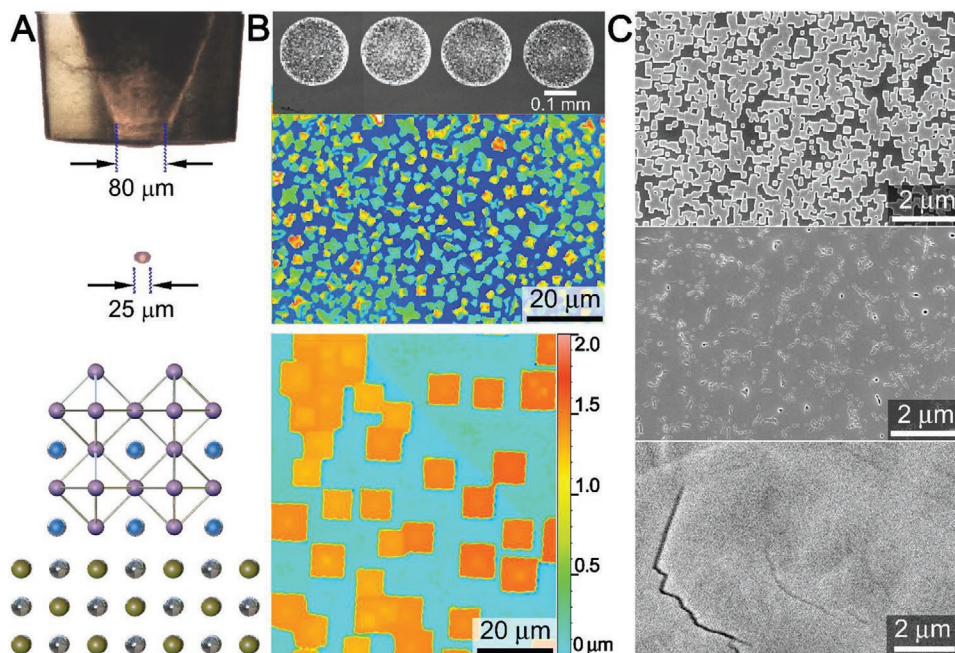

Figure 1. The role of substrate for inkjet printer CH$_3$NH$_3$PbBr$_3$ perovskites. A) Ejection of a single droplet from a piezoelectric driven glass nozzle with an orifice of 80 μm (top). Schematic interface between CH$_3$NH$_3$PbBr$_3$ perovskite and PbS having a cubic rock salt structure with a lattice mismatch ≈0.3% (violet = iodide, blue = CH$_3$NH$_3$, silver = lead, yellow = sulfur) (bottom). B) Printed structures on non-crystalline surfaces: glass (top), untreated GaAs (middle). Confocal optical microscope images of printed CH$_3$NH$_3$PbBr$_3$ microcubes exhibiting an epitaxial relation to the PbS substrate (bottom). C) Scanning electron microscope images, exhibiting samples with increasing amount of deposited material showing an evolution from cubic crystallites merged to islands, to closed film. The full film at (C-bottom) and the big crystallites in (B-bottom) were obtained at a humidity of 80%, whereas the structures in (b-middle, c-top and middle) were printed at 40% humidity.

distributed within the deposited droplet. The lateral dimensions were in the ≈10 µm range whereas a typical height of the perovskite structures was around 1.3 µm (Figure 1B bottom). While some of the crystallites merged to form extended islands, all of them exhibited the same orientation, which is a clear signature of epitaxial growth. The top facets of the cubes were parallel to the {100} oriented cleavage plane of the substrate and the side facets were parallel to the <100> oriented substrate edges. This orientation of the crystallites suggests coherent lattice of the MAPbBr$_3$ crystallites on top of the PbS substrate. Similarly, a coherent continuation of the crystal lattice across a MAPbI$_x$Br$_{3-x}$/PbS interface was observed before of colloidal PbS quantum dots embedded within a MAPbI$_x$Br$_{3-x}$ matrix.[43] The coherent interfaces have been the essence to achieve high quantum yields from infrared light emitting diodes,[43] as well as high responsivity and electron mobility for infrared quantum dot photodetectors[42] based on this material combination. In respect to the distribution of epitaxially grown rectangular structures on the substrate, the pattern presented at the bottom of Figure 1B are reminiscent to the case of NaCl on Ag/Au/Si(100), which was obtained by spin-casting from solution in ref. [34]. The advantages of inkjet printing are the material efficiency of the DOD ejection of picoliter amounts of solvents at predefined locations, and the facile control of the amount of material deposited at each sample position. By increasing the ejection rate, the density of cubic epitaxial islands was controlled (Figure 1C). At lower rate separate crystallites were generated which merged into islands. At higher rate, the crystallites were merged to a complete film, interrupted by a few holes, and covered by shallow trenches, which are both formed due to solvent vapors escaping from the film during drying. (Figure 1C middle). Under appropriately chosen deposition conditions (same ejection rate as the Figure 1C middle, but increased relative humidity of 80%), these imperfections could be avoided, and especially toward the edges of the printed lines, films with smooth surfaces were found (Figure 1C bottom, Figure S5a, Supporting Information) with a film thickness of more than 300 nm (Figure S5b, Supporting Information). The presence of the film on the substrate surface was detected by tiny cracks, continuously formed under the bombardment in the scanning electron microscope, or by traces of scratches produced into the film with plastic tweezers (Figure 1C, bottom, Figure S5, Supporting Information).

2.2. Photoluminescence and Lattice Anchoring

In spite of the lability of the perovskite layers under e-beam exposure[44] it is astonishing that the isolated cubic nanostructures provide cathodo-luminescence even at room temperature, and each of the cubes was found to be luminescent by comparison of panchromatic to secondary electron images (Figure S6, Supporting Information). The luminescence, as investigated under an optical microscope shows the typical signatures of MAPbBr$_3$. Even though the structures were grown on a semiconductor with a substantially smaller band gap, acting as carrier acceptor for photoexcited electrons and holes, the structures exhibited under laser excitation at 405 nm intense green luminescence (**Figure 2**A). The variously sized crystals exhibited variations in emission intensity from structure to structure
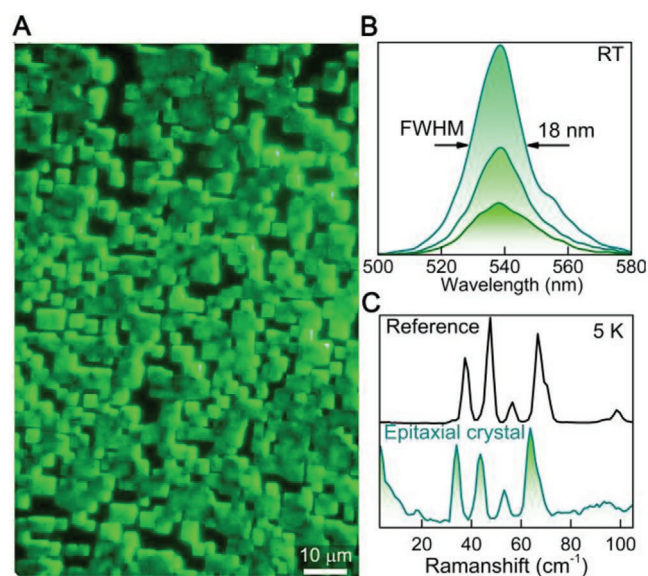

Figure 2. Optical properties of MAPbBr$_3$ epitaxial micro-cubes. A) Microscopic image of the luminescent structures under laser excitation at a wavelength of 405 nm. B) Room temperature spectra of three individual nanocubes. C) Low temperature (5 K) Raman spectrum at 633 nm excitation wavelength of a single microcube in comparison to that of a macroscopic reference single crystal.

and also within the cubes, however, each cube showed a peak emission at the same wavelength of 538 nm and approximately also the same linewidth of 18 nm (Figure 2B). This line width is narrower as compared to the line width of single crystals, grown for instance by inverse temperature crystallization method.[45]

The single crystalline nature of the epitaxial MAPbBr$_3$ structures obtained by ink-jet printing was confirmed also by micro-Raman spectroscopy, providing comparable spectra for the epitaxial structures and bulk reference samples (Figure 2C). The Raman peaks below 200 cm^{-1} are attributed to lattice vibrations of the PbBr^{3-} component. The spectra of the bulk single crystal sample are in good agreement with literature.[46,47] The Raman peaks of the cubic shaped epitaxial structures are slightly shifted to lower wavenumbers with respect to the reference single crystal. This might indicate strain in the epitaxial structure due to the PbS substrate. The temperature dependence of the Raman spectra (**Figure 3**) reveals various phase transitions of MAPbBr$_3$, from the low temperature orthorhombic phase to two different tetragonal phases and the cubic phase at room temperature. Spectroscopical evidence of the phase transition to the cubic phase is observed between 200 and 235 K in the reference single crystal, in accordance with literature (Figure 3A).[47,48] The epitaxial structures show similar spectral features of a phase transition at around 40 K lower temperature (Figure 3B, Figure S7, Supporting Information). This temperature shift of the phase transition might be due to a lattice anchoring effect due to the presence of the substrate, where the cubic lattice of the PbS is stabilizing the MAPbBr$_3$ structure. Similar lattice anchoring effects have been reported to occur when PbS quantum dots are embedded into a perovskite matrix, with the same lattice parameter as the quantum dots.[49] In that case, the lattice anchoring effect was substantially increasing the stability and lifetime of the perovskite material.
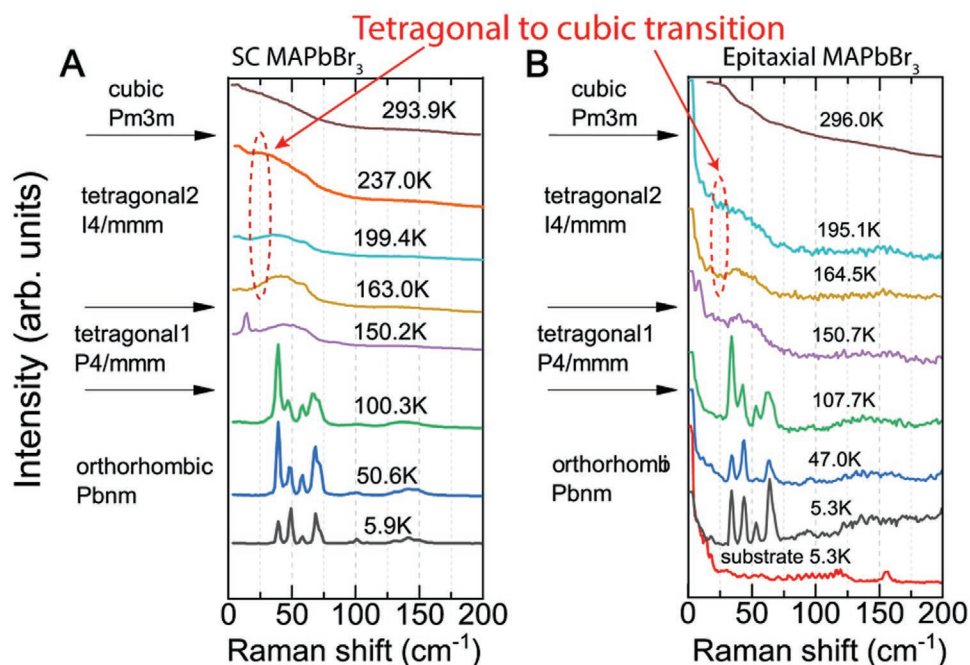
Figure 3. Phase transitions. Raman spectra of A) MAPbBr$_3$ single crystal (SC, left) and B) epitaxial structures on PbS (right) as function of temperature. Evidence of phase transitions is observed by changes of the spectral features. Phases of the single crystal are indicated according to ref. [47]. The red line on the right panel shows a reference spectrum of the PbS substrate.

Recently, similar anchoring effects have also been reported on solution grown formamidinium lead iodide FAPbI$_3$ on MAPbCl$_x$Br$_{3-x}$ single crystal substrates.[50]

2.3. Quenching Uncontrolled Crystallization

A key to obtain epitaxial growth is that the solid substrate surface acts as a seed for the attachment of precursor ions from solution in a way that the deposited material continues the atomic arrangement of the substrate. Nucleation and crystal growth can take place, however, also at other locations, considering that the used solvents, in particular DMSO support also single crystal growth from solutions by the inverse-temperature-crystallization process,[45] performed at similar temperatures as our substrate is kept during epitaxial growth. DMSO as well as DMF is known to form intermediates in solution with the precursors used for perovskite growth (PbI$_2$ and MAI).[51] Crystallization of intermediates in solution and on substrates, will result in rather uncontrolled crystal orientations and undesired crystal directions, which should be avoided, when optimized epitaxial metal halide perovskites are desired. As shown in the following, as a tool to reduce competitive crystallization of intermediates and thus optimized growth of perovskites environmental humidity can be used as control nob.

The closed films with smooth surfaces discussed above were obtained under high humidity of >80% (Figure 1C, bottom), and also the most perfect cubic structures where obtained at high humidity (Figure 1B, bottom). At lower humidity of 40% much smaller crystallite sizes were observed as well as complete films with holes and other surface damages (Figure 1C, top and middle). An even more drastic effect of humidity we

observed for the growth of MAPbI$_3$ on (111) oriented surfaces of PbTe substrates. In particular, ≈1 micrometer thick layers of PbTe, grown by conventional molecular beam epitaxy on cleaved surfaces of BaF$_2$ single crystalline substrate, were used. On these substrates at 40% humidity, elongated crystallites were grown, found in three orientations on the substrate. The needle like crystallites were elongated into the three <110> directions within the (111) plane, pointing parallel to the cleaving edges of the BaF$_2$ substrates (**Figure 4**A). The composition of the needles was proven by X-ray diffraction (XRD) to be that of MAPbI$_3$ with only small inclusions of PbI$_2$ (Figure S8a, Supporting Information). Pole figures of the 001 Bragg peak evidenced three different growth directions of the crystallites (Figure S8b, Supporting Information) but having one axis in common. The common axis is a [310] axis (in cubic notation) which is found to be perpendicular to the (111) oriented substrate surface. Thus, at the interface the <111> crystalline directions of the perovskite are tilted by an angle of 43.1° in respect to the [111] direction of the substrate. Thus, the top layer is of multi-crystalline nature and at the interface the lattice is disrupted, due to the lattice mismatch between the (111) oriented PbTe surface layer and the (310) oriented bottom layer of the MAPbI$_3$ perovskite (Figure 4B left, Figure S9, Supporting Information). By considering the interface energies between the MAPbI$_3$ and the PbTe we could not find any justification for the <310> growth directions of the MAPbI$_3$ on the (111) oriented PbTe surfaces. Thus, other possibilities had to be taken into account to explain the generation of this particular growth direction. A possible solution of this problem is provided by considering the so-called solvent engineering process for deposition of MAPbI$_3$, as was introduced by N. J. Jeon et al. to produce uniform and dense films.[52] In his process, the perovskite
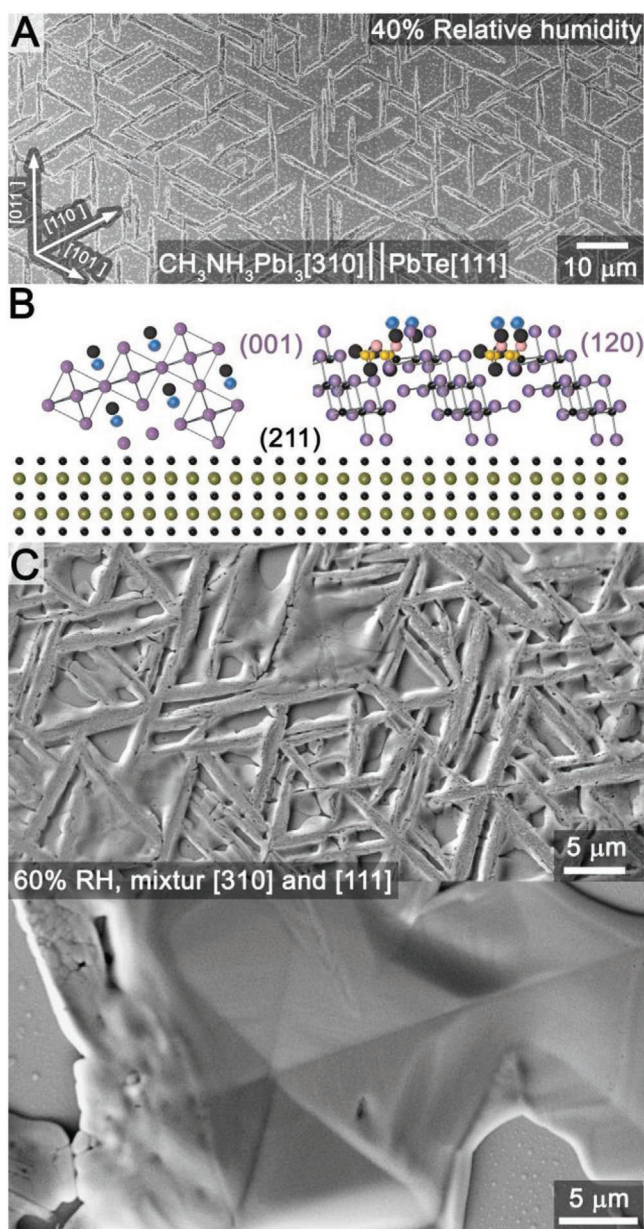
**ADVANCED
SCIENCE NEWS**

www.advancedsciencenews.com

**ADVANCED
FUNCTIONAL
MATERIALS**

www.afm-journal.de

Figure 4. Influence of humidity. A) MAPbI$_3$ on a (111) oriented surface, deposited at relative humidity of 40%, showing growth of oriented needles. B) Left: Sketch of the interface between [310] MAPbI$_3$ on a PbTe substrate. Shown is the (211) zone axis of the substrate. Right: Interface between the intermediate phase with intercalated DMSO molecules in between sheets of PbI$_2$. C) Scanning electron microscopy images of MAPbI$_3$ printed at elevated humidity of 60% on [111] oriented PbTe. In between the needles surfaces are partly covered by perovskites.

precursors are deposited from a solvent mixture containing DMSO on the substrate. After dropping a further solvent on the film during spin casting and removal of the solvent, an intermediate phase was formed. This intermediate phase was identified as MAI-PbI$_2$-DMSO, which was converted into a MAPbI$_3$ perovskite by a subsequent annealing step. The annealing was performed at 100 °C for 10 min, similar to the annealing step we used after deposition of the material by inkjet printing and

drying of the solvent. Considering the crystal structure of the intermediate phase, where the DMSO is separating PbI$_2$ sheets, an approximate lattice matching between the PbTe [111] plane and that of the intermediate phase can be found, when the PbI$_2$ sheets are tilted in respect to the interface (Figure 4B, right, Figure S9, Supporting Information). This indicates a scenario, that by the inkjet printing initially at the interface an intermediate phase was formed, which was converted during annealing by removal of the DMSO molecules in between the lead iodide layers. A recrystallization from the intermediate phase to the perovskite, however, without reorienting all the crystal planes, resulted finally in the oblique, [310] orientation of the MAPbI$_3$ on the [111] interface. Interestingly, this orientation of the MAPbI$_3$ was found to be metastable, and the MAPbI$_3$ showed on a time scale of days a conversion to crystallites with a [111] direction being perpendicular to the [111] oriented PbTe surface (Figure S10, Supporting Information). This observation underlines, that the [310] oriented perovskite crystallites are not the thermodynamic equilibrium case, but another orientation (MAPbI$_3$ [111]//PbTe[111]) would be more beneficial.

Increasing the humidity during deposition resulted in a drastically different crystallite growth. Above 60% humidity in addition to the needle shaped crystallite network the areas in between the needles were partially filled by MAPbI$_3$, exhibiting indications of crystallites with hexagonally shaped basis (Figure 4C). Above 80% humidity exclusively hexagonal prisms were obtained (**Figure 5**A). By optical confocal microscopy, the single hexagons were determined to be ≈2 µm high and their lateral extend varied (Figure 5B). Almost all the hexagons had a width exceeding 10 µm. The top surface of the prisms was parallel to the (111) substrate surface in the center of the hexagons. The center plateaus were surrounded by inclined facets, exhibiting an angle of 54.7° to the (111) plane, which indicated that these are oriented in <100> equivalent directions (Figure 5B). The compositions of the hexagons were confirmed to be MAPbI$_3$ by wide angle XRD spectra (Figure S11a, Supporting Information), evidencing only a small inclusion of PbI$_2$ phases. Also, these structures showed coherent interface to the substrate, which was visualized by the continuation of atomic rows in the cross-sectional transmission electron microscopy image (Figure 5C). A closer inspection of the TEM image and local electron diffraction spectra revealed the presence of PbI$_2$ at the interface to the PbS substrate. The PbI$_2$ could be formed during deposition and cause the orientation of the MAPbI$_3$ grown on top of it, or it could also be formed due to damage during lamella preparation by a focused ion beam or under the intense electron radiation of the TEM, as is suggested in ref. [44]. All hexagons exhibited the same orientation in lateral direction and the pole figure, performed for the 110 Bragg reflection of MAPbI$_3$, confirmed the growth direction of the hexagons to be a [111] direction (in cubic notation) (Figure S11b, Supporting Information). This brings us to the conclusion, that the humidity results in addition of water to the DMSO based solution, at least after ejection of the micron sized droplets form the inkjet nozzle. An effect of water addition is that intermediate phases of PbI^{2-}DMSO–MAI, which are reported to be formed in solution,[51] subsequently forming the intermediate phases in the deposited films, are effectively quenched (Figure S12a,b, Supporting Information). Furthermore, the boiling point of the
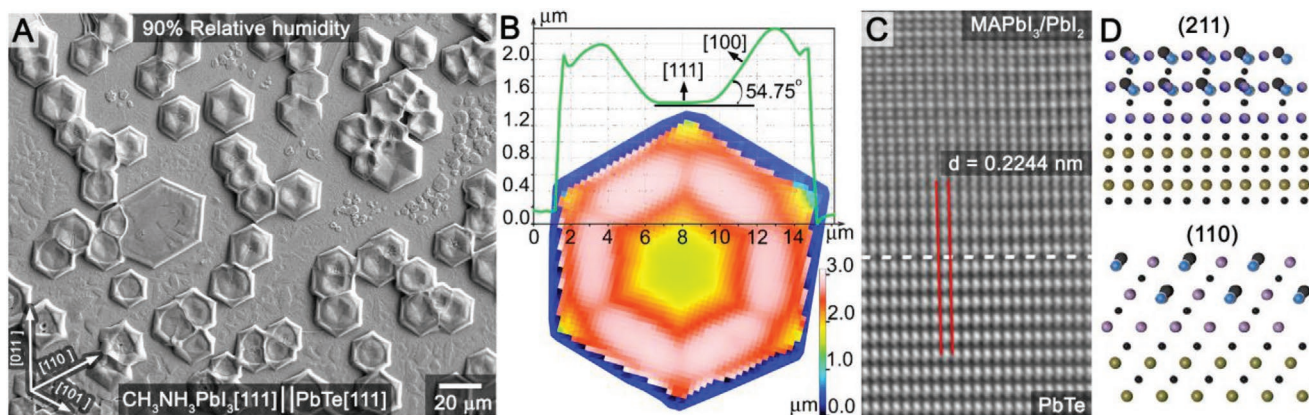
Figure 5. Growth at high humidity. A) At a relative humidity of 90% hexagonal platelets of MAPbI₃ are grown on PbTe [111]. B) Confocal optical microscope image of a single hexagonal perovskite platelet on PbTe [111] together with a height profile. C) High-resolution cross-sectional transmission electron image of a MAPbI₃ or a PbI₂/PbTe interface, exhibiting a coherent continuation of the atomic lattice planes. D) Sketch of the MAPbI₃/PbTe interface for two zone axes, [211] and [110].

solvent mixture is reduced (Figure S12c, Supporting Information).[53] Thus at the substrate temperature used for the inkjet printing, the DMSO evaporation was accelerated and no metastable intermediate phase was formed. The direct growth resulted in an orientation of the crystallites, provided by the lattice match between the [111] oriented PbTe surface and that of the MAPbI₃ (Figure 5D) and the concomitant interface energy minimization. Thus, quenching the intermediates in the DMSO/DMF solution promotes epitaxial growth on the substrates surface, and allows the formation of well-ordered crystallites (Figure 5A) and closed epitaxial films (Figure 1C).

2.4. Epitaxial CsPbHal3 on Various Substrates

In history, the Pb-chalcogenides used as substrates in the studies above acted most importantly as pioneering materials for fundamental investigations. PbS, in particular, was the first material for which any semiconducting properties had been observed already in 1822.[54] Similarly, epitaxial PbTe has been a key in the demonstration of first 3D quantum dot crystals ever grown.[55] Later on, the fundamental insights gained from the Pb-chalcogenides were transferred to other semiconductors such as silicon and III/V compounds semiconductors, which are nowadays prevailing in electronics. A similar development can be expected for the epitaxial growth by inkjet printing, which is by no means restricted to lead-containing chalcogenides or lead-containing metal halide perovskites. To propose alternative substrate materials, which are readily available either from natural sources or from large scale production, in the following, we tested several more substrate/epistructure material combinations. Naturally available crystals often used as test-substrates for epitaxial growth is Muscovite mica, which allows a "Van der Waals" type of epitaxial growth.[56] As a possible second material provides by nature, we used FeS₂ (pyrite, also called "Fools Gold") as a crystalline substrate, providing a cubic lattice with a lattice spacing of 5.4 Å.[57] A most crucial substrate frequently used is GaAs, which would allow the integration of perovskite epitaxial structures to conventional optoelectronic devices. For comparison, the growth

of CsPbBr₃ on [100] PbSnSe is demonstrated, which acts as a favorable substrate due to its similar spacing distances and surface atom arrangement to the perovskite. The experiments were performed with CsPbCl₃ and CsPbBr₃, due to their similar lattice constants as compared to those of the substrates (except of mica). As the Pb-chalcogenide substrates described above, GaAs and PbSnSe, and the natural crystal FeS₂ substrates with [100] interfaces were treated with Br₂-methanol solutions for surface activation, whereas for the muscovite mica the substrate was freshly cleaved to obtain clean surfaces. After deposition on all of these four substrates we found areas within the deposited droplets, where well faceted crystallites were formed. Within these areas the crystallites had also an orientation which was related to that of the substrates. On Fools Gold and on PbSnSe we found the [100] facets of the CsPbCl₃ and CsPbBr₃, respectively, to be parallel to the [100] of the substrates, evidencing epitaxial growth (**Figure 6**A,B). On mica, three orientations of the crystallites were found (Figure 6C), which is similar to the case of metal halide perovskites structures grown previously by chemical vapor deposition methods,[58] and is explained by the hexagonal arrangement of surface atoms on the mica cleavage plane. The three orientations of the crystallites are confirmed unambiguously by the Fourier transform image shown in the inset of Figure 6c. Most importantly, however, on GaAs substrate also epitaxial growth of CsPbBr₃ was achieved. Our first attempt showed close to cubic shaped crystallites with two orientations (Figure 6D). In addition to those exhibiting their edges in parallel to that of the substrate also crystallites oriented in the [110] direction of the substrate were observed. While these results are a first step in direction of epitaxial growth from solutions by inkjet printing on GaAs, further improvements are required in order to obtain a thin film with controlled thickness. These improvements might include: i) Attempts to obtain a better lattice match between the perovskite and GaAs by using lattice tuning of mixed halide perovskites, ii) since GaAs has very different chemical properties as lead chalcogenides, a different surface activation process might be needed, iii) changing the environment from air to inert atmosphere or even better to vacuum, to avoid an instantaneous formation of a surface oxide layer on the GaAs which is amorphous.
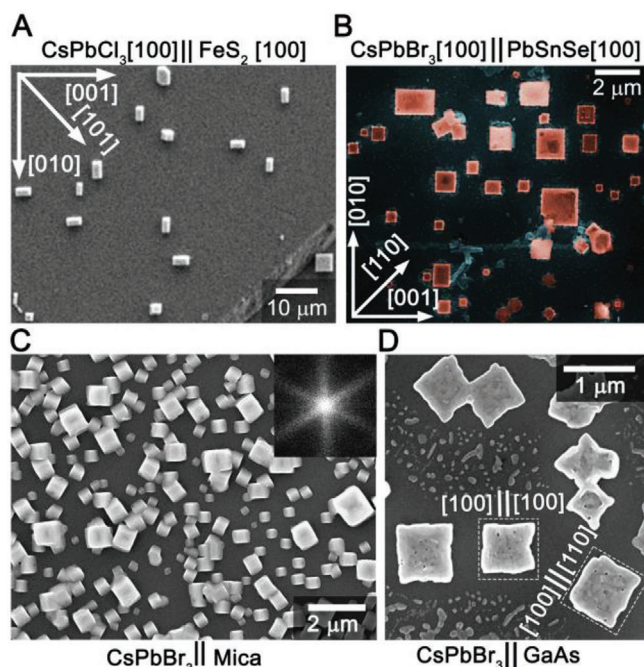
**ADVANCED
SCIENCE NEWS**
www.advancedsciencenews.com

**ADVANCED
FUNCTIONAL
MATERIALS**
www.afm-journal.de

Figure 6. Various substrates. A) CsPbCl₃ and B) CsPbBr₃ epitaxial growth on natural (FeS₂, mica) and commonly used substrates (GaAs). Growth on PbSnSe [100] is shown for comparison. The substrates were either activated by bromination or freshly cleaved to obtain clean surfaces, enabling epitaxial growth. The material/substrate combinations are described in the figure. The Fast Fourier Transform of image (C) shown in the inset highlights the orientation of the crystallites on Mica substrate into three distinct directions.

3. Conclusion

The ordered micro- and nanostructures and their evolution form separate islands to a complete closed film as described above, evidence an epitaxial growth of solution processed metal halide perovskites on various substrates. The growth mode of heteronucleation of islands followed by a subsequent merging to an epitaxial layer is similar than what is observed in standard liquid phase epitaxy of conventional inorganic semiconductors, where materials are grown from a melt at high temperatures. In contrasts to the standard liquid phase epitaxy for the epitaxy of the perovskite solutions, extremely low substrate temperatures are sufficient to achieve the desired ordered growth of a single crystalline material on top of a substrate. The deposition of the liquids by an inkjet printer was found here to be very cost and materially economic, and in a simple way several perovskite/substrate combinations were tested. As for conventional epitaxial growth, there are a set of crucial parameters to be adjusted, to obtain crystalline structures and films. Humidity, surface activation, substrate temperature are the most important to be listed besides the choice of the substrate. For the lead-halide perovskites investigated here, lead chalcogenides seem to be the best choice, which are not commonly available in the form of large wafers. However, they can be prepared by molecular beam epitaxy, even on substrates such as silicon. Thus, a combination perovskite epitaxy from inkjet printing with and epitaxial lift off process, which allows multiply use of the substrates, could allow also fabrication of epitaxial structures in large scale. This will enable the development of scalable single-crystal, LEDs, lasers, X-ray detectors and solar cells, with optimized performances in respect to the commonly used polycrystalline structures, currently produced by solution processing. While the work here was restricted to the archetypical MAPbX3 and CsPbHal3 halide perovskites, the epitaxy by inkjet printing is certainly also a good option for further perovskite and non perovskite based ionic semiconductors, and insulators as a versatile platform for organic/inorganic (opto-)electronic devices with the advantages of single crystal materials.

4. Experimental Section

Chemicals: Lead chloride, lead bromide, lead iodide, caesium chloride, caesium bromide, hydrochloric acid in water, hydrobromic acid in water, methylamine solution in ethanol, bromine, methanol, ethanol, DMSO, DMF were obtained from Sigma-Aldrich and Alfa Aesar and were used without purification. Methylammonium bromide and iodide were synthesized by mixing methylamine solution with appropriate acid according previously published methods.[59]

Substrates: Single crystals of lead sulfide (PbS) were grown by self-selecting vapor growth method.[60] Substrates were cleaved from single crystals with razor blade along crystallographic planes (100). The <111> oriented lead telluride on barium fluoride, <100> oriented lead telluride on potassium chloride, <100> oriented lead-tin selenide on sodium chloride were grown by molecular beam epitaxy. Gallium arsenide wafers were purchased from University Wafer. Iron disulfide (pyrite) and muscovite mica were purchased from commercial suppliers.

Substrate Activation: Lead sulfide single crystal, lead telluride, lead-tin selenide, gallium arsenide, iron disulfide were activated 5 min prior to the printing experiments. For activation, the substrates were dipped into a 0.125 mass% bromine/methanol solution for 5 s and then was washed two times by dipping into pure methanol. The substrates were dried by blowing solution rests off with compressed air. Muscovite mica was freshly cleaved before printing.

Printing: The perovskite ink was prepared by mixing stoichiometric amounts of methyl-ammonium halides or caesium halides with appropriate lead halides, to achieve a 0.25 M concentration in DMF/DMSO mixture with a volume ration of 3 to 1. The printing substrate stage was preheated to 80 °C surface temperature. The substrate was placed after the activation step to the stage and was kept for 1–2 min to allow the substrate to reach the desired surface temperature. The printed samples were transferred into a nitrogen filled glove box and were annealed at 100 centigrade for 1 h. The perovskite inks were printed in a setup including a single MJ-AT printing nozzle (Microfab Technologies) with an 80 µm orifice. For droplet monitoring, stroboscopic illumination by a light-emitting diode was used, synchronized to the pulses applied to the piezoelectric print head. The substrate was moved by a motorized translation stage (Standa, 8MT173) and a step size of 1.25 µm. Stable drop ejection was achieved by proper selection of the electrical drive parameter for the piezo jetting device (applied was a trapezoidal shaped double-pulse with an amplitude of +80 V, a dwell time of 6 µs, and rise and fall times of 4 µs). Pattern formation on the glass substrates was controlled by adjusting the printing frequency from 5 till 40 Hz at constant stage speed (5 mm s⁻¹). The substrate temperature was controlled by a heater coupled with a thermos-controller.

Electron Microscopy: Field-emission scanning-electron-microscopy was performed with a JEOL 7610F instrument. With this instrument also panchromatic cathodoluminescence in the spectral range of 400–1200 nm was carried out at room temperature, by making use of Deben Centaurus detector. Electron energies up to 20 keV were applied as excitation. Lamellae for structural characterization were prepared with a standard lift-out technique using a Helios Nanolab 660 dual beam FIB/SEM system from FEI Company. The high-resolution transmission electron microscopy was performed with a Titan Themis3 300 (FEI

Company, Hillsboro, USA) instrument, equipped with a high-brightness field-emission gun operated at an accelerating voltage of 200 kV.

Optical Microscopy: A confocal microscope from NanoFocus was used to measure height profiles from printed epitaxial perovskite crystals. An IMA fluorescence microscope was equipped with a hyper spectral camera was used for imaging of epitaxial perovskites together with photoluminescence measurements at selected spots under back continuous wave back side illumination with a with 405 nm laser.

Spectroscopy: Raman spectroscopy was performed with a LabRAM microscopeHR800 spectrometer (Horiba Jobin Yvon) with an excitation wavelength of 6332.816 nm. Measurements were taken at temperatures between 4K-300K and pressure of around 10−6 mbar in an OXFORD-CryoOxford Microstat-He. XPS measurements were performed at a commercially available PHI Quantera II machine equipped with a monochromated Al Kα X-ray source (1486.6 eV) and a multi-channel electron detector. Argon sputtering (2 kV, 1 min) was used to remove the topmost layers (≈10 nm).

Supporting Information

Supporting Information is available from the Wiley Online Library or from the author.

Conflict of Interest

The authors declare no conflict of interest.

[1] C. R. Kalaiselvi, N. Muthukumarasamy, D. Velauthapillai, M. Kang, T. S. Senthil, *Mater. Lett.* **2018**, *219*, 198.

[2] P. Meredith, A. Armin, *Nat. Commun.* **2018**, *9*, 8.

[3] M. A. Green, A. Ho-Baillie, H. J. Snaith, *Nat. Photonics* **2014**, *8*, 506.

[4] See, for example, the date for perovskite solar cells in the chart reporting best research cell efficiencies from NREL, https://www.nrel.gov/pv/insights/assets/pdfs/cell-pv-eff-emergingpv.pdf (accessed: July 2020).

[5] N. J. Jeon, J. H. Noh, W. S. Yang, Y. C. Kim, S. Ryu, J. Seo, S. I. Seok, *Nature* **2015**, *517*, 476.

[6] M. Saliba, T. Matsui, J. Y. Seo, K. Domanski, J. P. Correa-Baena, M. K. Nazeeruddin, S. M. Zakeeruddin, W. Tress, A. Abate, A. Hagfeldt, M. Grätzel, *Energy Environ. Sci.* **2016**, *9*, 1989.

[7] D. W. de Quilettes, S. M. Vorpahl, S. D. Stranks, H. Nagaoka, G. E. Eperon, M. E. Ziffer, H. J. Snaith, D. S. Ginger, *Science* **2015**, *348*, 683.

[8] W. Li, J. Fan, J. Li, Y. Mai, L. Wang, *J. Am. Chem. Soc.* **2015**, *137*, 10399.

[9] Y. Hou, X. Du, S. Scheiner, D. P. McMeekin, Z. Wang, N. Li, M. S. Killian, H. Chen, M. Richter, I. Levchuk, N. Schrenker, E. Spiecker, T. Stubhan, N. A. Luechinger, A. Hirsch, P. Schmuki, H. P. Steinrück, R. H. Fink, M. Halik, H. J. Snaith, C. J. Brabec, *Science* **2017**, *358*, 1192.

[10] Z. Chen, B. Turedi, A. Y. Alsalloum, C. Yang, X. Zheng, I. Gereige, A. AlSaggaf, O. F. Mohammed, O. M. Bakr, *ACS Energy Lett.* **2019**, *4*, 1258.

[11] X. Cheng, S. Yang, B. Cao, X. Tao, Z. Chen, *Adv. Funct. Mater.* **2020**, *30*, 1905021.

[12] C. Ji, S. Wang, Y. Wang, H. Chen, L. Li, Z. Sun, Y. Sui, S. Wang, J. Luo, *Adv. Funct. Mater.* **2020**, *30*, 1905529.

[13] Y. Liu, Y. Zhang, Z. Yang, D. Yang, X. Ren, L. Pang, S. Liu, *Adv. Mater.* **2016**, *28*, 9204.

[14] Y. Liu, Q. Dong, Y. Fang, Y. Lin, Y. Deng, J. Huang, *Adv. Funct. Mater.* **2019**, *29*, 1807707.

[15] W. Wei, Y. Zhang, Q. Xu, H. Wei, Y. Fang, Q. Wang, Y. Deng, T. Li, A. Gruverman, L. Cao, J. Huang, *Nat. Photonics* **2017**, *11*, 315.

[16] W. Peng, L. Wang, B. Murali, K. T. Ho, A. Bera, N. Cho, C. F. Kang, V. M. Burlakov, J. Pan, L. Sinatra, C. Ma, W. Xu, D. Shi, E. Alarousu, A. Goriely, J. H. He, O. F. Mohammed, T. Wu, O. M. Bakr, *Adv. Mater.* **2016**, *28*, 3383.

[17] Z. Chen, Q. Dong, Y. Liu, C. Bao, Y. Fang, Y. Lin, S. Tang, Q. Wang, X. Xiao, Y. Bai, Y. Deng, J. Huang, *Nat. Commun.* **2017**, *8*, 1890.

[18] X. D. Wang, W. G. Li, J. F. Liao, D. B. Kuang, *Sol. RRL* **2019**, *3*, 1800294.

[19] Q. Dong, Y. Fang, Y. Shao, P. Mulligan, J. Qiu, L. Cao, J. Huang, *Science* **2015**, *347*, 967.

[20] Y. X. Chen, Q. Q. Ge, Y. Shi, J. Liu, D. J. Xue, J. Y. Ma, J. Ding, H. J. Yan, J. S. Hu, L. J. Wan, *J. Am. Chem. Soc.* **2016**, *138*, 16196.

[21] L. Lee, J. Baek, K. S. Park, Y. E. K. Lee, N. K. Shrestha, M. M. Sung, *Nat. Commun.* **2017**, *8*, 15882.

[22] L. Goldstein, F. Glas, J. Y. Marzin, M. N. Charasse, G. Le Roux, *Appl. Phys. Lett.* **1985**, *47*, 1099.

[23] B. S. Meyerson, K. J. Uram, F. K. LeGoues, *Appl. Phys. Lett.* **1988**, *53*, 2555.

[24] D. J. Ashen, P. J. Dean, D. T. J. Hurle, J. B. Mullin, A. M. White, P. D. Greene, *J. Phys. Chem. Solids* **1975**, *36*, 1041.

[25] B. S. Meyerson, *Appl. Phys. Lett.* **1986**, *48*, 797.

[26] H. Amano, N. Sawaki, I. Akasaki, Y. Toyoda, *Appl. Phys. Lett.* **1986**, *48*, 353.

[27] L. Wang, P. Chen, N. Thongprong, M. Young, P. S. Kuttipillai, C. Jiang, P. Zhang, K. Sun, P. M. Duxbury, R. R. Lunt, *Adv. Mater. Interfaces* **2017**, *4*, 1701003.

[28] J. Jiang, X. Sun, X. Chen, B. Wang, Z. Chen, Y. Hu, Y. Guo, L. Zhang, Y. Ma, L. Gao, F. Zheng, L. Jin, M. Chen, Z. Ma, Y. Zhou, N. P. Padture, K. Beach, H. Terrones, Y. Shi, D. Gall, T.-M. Lu, E. Wertz, J. Feng, J. Shi, *Nat. Commun.* **2019**, *10*, 4145.

[29] Y. Wang, Y. Shi, G. Xin, J. Lian, J. Shi, *Cryst. Growth Des.* **2015**, *15*, 4741.

[30] J. Chen, D. J. Morrow, Y. Fu, W. Zheng, Y. Zhao, L. Dang, M. J. Stolt, D. D. Kohler, X. Wang, K. J. Czech, M. P. Hautzinger, S. Shen, L. Guo, A. Pan, J. C. Wright, S. Jin, *J. Am. Chem. Soc.* **2017**, *139*, 13525.

[31] L. Ji, H. Y. Hsu, J. C. Lee, A. J. Bard, E. T. Yu, *Nano Lett.* **2018**, *18*, 994.

ADVANCED
SCIENCE NEWS

www.advancedsciencenews.com

ADVANCED
FUNCTIONAL
MATERIALS

www.afm-journal.de

[32] M. V. Kelso, N. K. Mahenderkar, Q. Chen, J. Z. Tubbesing, J. A. Switzer, *Science* **2019**, *364*, 166.

[33] D. Angmo, T. T. Larsen-Olsen, M. Jørgensen, R. R. Søndergaard, F. C. Krebs, *Adv. Energy Mater.* **2013**, *3*, 172.

[34] J. S. Yu, I. Kim, J. S. Kim, J. Jo, T. T. Larsen-Olsen, R. R. Søndergaard, M. Hösel, D. Angmo, M. Jørgensen, F. C. Krebs, *Nanoscale* **2012**, *4*, 6032.

[35] H. Sirringhaus, T. Kawase, R. H. Friend, T. Shimoda, M. Inbasekaran, W. Wu, E. P. Woo, *Science* **2000**, *290*, 2123.

[36] T. N. Ng, B. Russo, B. Krusor, R. Kist, A. C. Arias, *Org. Electron.* **2011**, *12*, 2012.

[37] V. Dua, S. P. Surwade, S. Ammu, S. R. Agnihotra, S. Jain, K. E. Roberts, S. Park, R. S. Ruoff, S. K. Manohar, *Angew. Chem., Int. Ed.* **2010**, *49*, 2154.

[38] H. Andersson, A. Manuilskiy, T. Unander, C. Lidenmark, S. Forsberg, H. E. Nilsson, *IEEE Sens. J.* **2012**, *12*, 1901.

[39] W. Wang, Y. W. Su, C. Chang, *Sol. Energy Mater. Sol. Cells* **2011**, *95*, 2616.

[40] T. M. Eggenhuisen, Y. Galagan, A. Biezemans, T. M. Slaats, W. P. Voorthuijzen, S. Kommeren, S. Shanmugam, J. P. Teunissen, A. Hadipour, W. J. Verhees, S. C. Veenstra, M. J. Coenen, J. Gilot, R. Andriessen, W. A. Groen, *J. Mater. Chem. A* **2015**, *3*, 7255.

[41] H. Minemawari, T. Yamada, H. Matsui, J. Tsutsumi, S. Haas, R. Chiba, R. Kumai, T. Hasegawa, *Nature* **2011**, *475*, 364.

[42] M. Sytnyk, S. Yakunin, W. Schöfberger, R. T. Lechner, M. Burian, L. Ludescher, N. A. Killilea, A. A. YousefiAmin, D. Kriegner, J. Stangl, H. Groiss, W. Heiss, *ACS Nano* **2017**, *11*, 1246.

[43] X. Gong, Z. Yang, G. Walters, R. Comin, Z. Ning, E. Beauregard, V. Adinolfi, O. Voznyy, E. H. Sargent, *Nat. Photonics* **2016**, *10*, 253.

[44] S. Chen, X. Zhang, J. Zhao, Y. Zhang, G. Kong, Q. Li, N. Li, Y. Yu, N. Xu, J. Zhang, K. Liu, Q. Zhao, J. Cao, J. Feng, X. Li, J. Qi, D. Yu, J. Li, P. Gao, *Nat. Commun.* **2018**, *9*, 4807.

[45] M. I. Saidaminov, A. L. Abdelhady, B. Murali, E. Alarousu, V. M. Burlakov, W. Peng, I. Dursun, L. Wang, Y. He, G. Maculan, A. Goriely, T. Wu, O. F. Mohammed, O. M. Bakr, *Nat. Commun.* **2015**, *6*, 7586.

[46] A. M. A. Leguy, A. R. Goñi, J. M. Frost, J. Skelton, F. Brivio, X. Rodríguez-Martínez, O. J. Weber, A. Pallipurath, M. I. Alonso, M. Campoy-Quiles, M. T. Weller, J. Nelson, A. Walsh, P. R. F. Barnes, *Phys. Chem. Chem. Phys.* **2016**, *18*, 27051.

[47] O. Yaffe, Y. Guo, L. Z. Tan, D. A. Egger, T. Hull, C. C. Stoumpos, F. Zheng, T. F. Heinz, L. Kronik, M. G. Kanatzidis, J. S. Owen, A. M. Rappe, M. A. Pimenta, L. E. Brus, *Phys. Rev. Lett.* **2017**, *118*, 136001.

[48] K. Nakada, Y. Matsumoto, Y. Shimoi, K. Yamada, Y. Furukawa, *Molecules* **2019**, *24*, 626.

[49] M. Liu, Y. Chen, C. S. Tan, R. Quintero-Bermudez, A. H. Proppe, R. Munir, Ha. Tan, O. Voznyy, B. Scheffel, G. Walters, A. P. T. Kam, B. Sun, M. J. Choi, S. Hoogland, A. Amassian, S. O. Kelley, F. P. G. de Arquer, E. H. Sargent, *Nature* **2019**, *570*, 96.

[50] Y. Chen, Y. Lei, Y. Li, Y. Yu, J. Cai, M. H. Chiu, R. Rao, Y. Gu, C. Wang, W. Choi, H. Hu, C. Wang, Y. Li, J. Song, J. Zhang, B. Qi, M. Lin, Z. Zhang, A. E. Islam, B. Maruyama, S. Dayeh, L. J. Li, K. Yang, Y. H. Lo, S. Xu, *Nature* **2020**, *577*, 209.

[51] M. Jung, S. G. Ji, G. Kim, S. I. Seok, *Chem. Soc. Rev.* **2019**, *48*, 2011.

[52] N. J. Jeon, J. H. Noh, Y. C. Kim, W. S. Yang, S. Ryu, S. I. Seok, *Nat. Mater.* **2014**, *13*, 897.

[53] The binary vapor–liquid equilibrium isobaric P-T-X-Y data for dimethylsulfoxide and water at a pressure of 550 mmHg ate taken from the Chemical Engineering Research Information Center, https://www.cheric.org/research/kdb/hcvle/showvle.php?vleid=511 (accessed: July 2020).

[54] T. J. Seebeck, Magnetische Polarisation der Metalle und Erze durch Temperatur-Differenz (Ed: A. J. V. Oettinger), W. Engelmann, Leipzig **1895**.

[55] G. Springholz, V. Holy, M. Pinczolits, G. Bauer, *Science* **1998**, *282*, 734.

[56] Q. Wang, M. Safdar, K. Xu, M. Mirza, Z. Wang, J. He, *ACS Nano* **2014**, *8*, 7497.

[57] R. Sun, G. Ceder, *Phys. Rev. B* **2011**, *84*, 245211.

[58] J. Chen, Y. Fu, L. Samad, L. Dang, Y. Zhao, S. Shen, L. Guo, S. Jin, *Nano Lett.* **2017**, *17*, 460.

[59] S. Yakunin, M. Sytnyk, D. Kriegner, S. Shrestha, M. Richter, G. J. Matt, H. Azimi, C. J. Brabec, J. Stangl, M. V. Kovalenko, W. Heiss, *Nat. Photonics* **2015**, *9*, 444.

[60] A. Szczerbakow, K. Durose, *Prog. Cryst. Growth Charact. Mater.* **2005**, *51*, 81.